FIS2005 http://www.mdpi.org/fis2005

Feynman-Hibbs Quantum Effective Potentials For Molecular Dynamic Simulations of Liquid Neon

N. Tchouar[*], M. Benyettou[*] and S.Benyettou[*]

Laboratory of Modelisation of Industrial Systems, Faculty of Science, U.S.T.O, P.O.Box BP 1505 El Menaour, Oran-Algeria. Fax : 21341420680. e-mail: tchouar@univ-usto.dz

Abstract: The quantum characteristics of liquid neon at two state points have been studied by means of molecular dynamics simulations involving effective pair potentials arising from the path-integral formalism, namely the quadratic Feynman-Hibbs potentials (QFH). Results include thermodynamics, structural and transport properties for the QFH and the classical Lennard-Jones models. The data reported in the paper are also compared, where possible, with available experimental information.

1. Introduction

Systems of spherical molecules, such as the rare gases, have been intensively studied over a broad range of temperatures and densities using pair interactions of Lennard-Jones (LJ) type. Extensive calculations of the equation of state of the LJ fluid have been performed with Monte Carlo (MC) and molecular dynamics (MD) numerical simulations [1]. LJ systems which present quantum effects have also been studied by computer simulations based on the Feynman path integral expression of the quantum canonical partition function. Quantum effects force liquid neon to disobey the law of corresponding states [2], although they are not so large as to make quantum exchange play a dramatic role in its behaviour [3]. So far, a number of computer simulations of this system has been performed by using different approaches : path-integral Monte Carlo (PIMC)[4-6], path-integral Brownian dynamics (PIBD) [7,8], semiclassical molecular dynamics with Gaussian wavepackets [8,9], semiclassical simulations based on the Wigner-Kirkwood asymptotic expansion in powers of ħ [10,11] and on the Feynman-Hibbs (FH) potentials [4,8], and perturbation theory plus simulation [12].
The path-integral formalism gives rise to the quadratic Feynman-Hibbs (QFH) quantum effective potentials. These model can be used easily in computer simulation schemes for studying the thermodynamical and structural properties of LJ systems such as neon, methane, and nitrogen [13,14]. More recently, the QFH potential has been applied to the study of light and heavy water by Guillot and Guissani [15].
The aim of this paper is to study the reliability of QFH potentials to predict quantum features of the liquid phase at condition far from exchange. As a probe, liquid neon has been studied at two state points. The calculations cover thermodynamic, transport properties and pair distribution functions.

2. Quadratic Feynman-Hibbs potential (QFH)

From the path-integral quantum partition function (without exchange) for a canonical ensemble (N, V, T) of atoms, and after some algebra, the Feynman-Hibbs (FH) potentials can be obtained. By keeping quadratic fluctuations around the classical path one obtains the QFH potential [16]:

$$U_{QFH}(r) = U_C(r) + \frac{\beta\hbar^2}{24\mu}\left[U_C{}''(r) + 2\frac{U_C{}'(r)}{r}\right] \qquad (1)$$

This potential is built so as to improve upon a classical interaction model C, normally Lennard-Jones (LJ), by taking into account factors related to quantum features (ħ, particle mass m = 2 μ, temperature T $=1/k_B\beta$). In figure 1, it is worthwhile to point out that at distances $r \leq r_m$ (LJ-minimum) the repulsive character of the potentials follows the ordering LJ < QFH, the difference being more pronounced as r and T decrease [17].
As regards the thermodynamics given by the effective potentials, some discrepancies from the classical formulae are expected [18]. In what follows, pointed brackets stand for the canonical average. The energy is given by:

$$E = \frac{3Nk_BT}{2} + \left\langle \beta \sum_{i<j} \frac{\partial U_{QFH}(r_{ij})}{\partial \beta} \right\rangle + \left\langle \sum_{i<j} U_{QFH}(r_{ij}) \right\rangle \qquad (2)$$

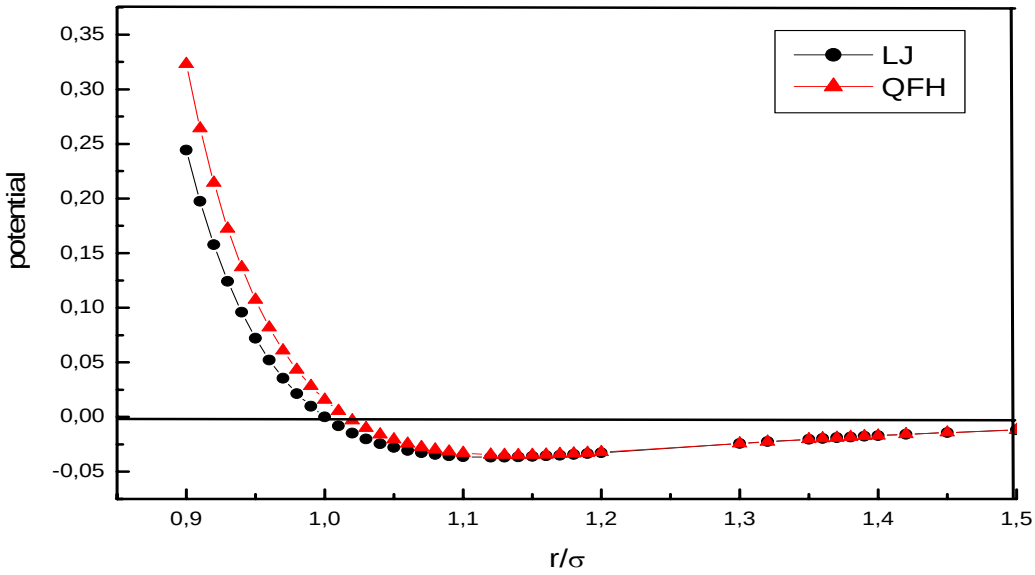

Figure 1: Interaction potential versus r/σ : black line and filled circle: LJ potential, red line and triangle: QFH potential. The plot corresponds to liquid neon at sp1 ($\rho^* = 0.6877$, $T^*=0.9517$).

where the second term (KEC) on the right-hand side can be interpreted as a quantum correction to the classical kinetic energy. The pressure equation remains, however, formally unchanged, because these potentials do not depend upon the liquid density ρ = N/V:

$$P = \frac{Nk_BT}{V} - \frac{1}{3V}\left\langle \sum_{i<j} r_{ij} \frac{\partial U_{QFH}(r_{ij})}{\partial r_{ij}} \right\rangle \qquad (3)$$

At a fixed value for temperature, in MC simulations, the quantum effects at the second order in ħ are taken into account by substituting the pair potential $U_C(r)$ by the $U_{QFH}(r)$. MD simulations, equivalent to MC simulations made with a QFH potential, are easily realized by using a MD simulation method at constant T where the value of β appearing in the QFH potential must be chosen consistently with T. It is clear that the estimate of the quantum effects by the QFH potential is only valid when the quantum corrections to classical quantities stay small. The order of magnitude of these corrections is given by the value of the parameter ($2\beta\,\hbar^2/\,m\sigma^2$) where σ is a typical length associated to the size of system molecules or atoms, for instance, equal to the σ parameter of the LJ potential modelling the interactions. In table 1, the values of this parameter are given for the studied liquid neon at the considered values of T. From these values, the next term in the expansion of the QFH potential of the order of ($2\beta\,\hbar^2/\,m\sigma^2$) is expected to be two order of magnitude smaller than the first order term.

3. Computational details

LJ and QFH molecular dynamics simulations have been performed with canonical ensemble, with a sample size N_s = 5324 particles in a cubic box surrounded by the usual toroidal boundary conditions [19]. The particle mass is m = 20.183 a.m.u and the basic LJ potential parameters for neon have been taken from the work by Morales and Singer [7], ε/k_B =36.83K, σ = 2.789 A°. A spherical cut-off potential truncation at half the box length has been employed in all simulations. The units of energy, length , and mass were chosen to be, repectively, ε, σ and m. The corresponding time unit is $\tau = \left(m\sigma^2/\varepsilon\right)^{1/2}$. The thermodynamical state of the system is specified through the reduced density and temperature $\rho^* = \rho\sigma^3$ and $T^* = k_B T/\varepsilon$. The simulations were carried out at constant volume and temperature using the Verlet algorithm and Hoover's thermostatting method [19], with the time step $\Delta t = 0.005\tau$. The two state points selected have been sp1 (ρ^* = 0.6877, T^*=0.9517) and sp2 (ρ^* = 0.6938, T^*=0.9792), and their ρ, T data have been taken from the work by Singer and Smith [5].
By using the Einstein formula, the diffusion coefficients *D* is obtained from the time dependent mean-square displacement of the molecules, expected linear at large time,

$$D = \lim_{t\to\infty} \frac{1}{6tN} \sum_{i=1,N} \left\langle \left| \mathrm{r_i}(t) - \mathrm{r_i}(0) \right|^2 \right\rangle \qquad (4)$$

where $\mathbf{r_i}(t)$ are the positions of the particles at time t. The shear viscosity coefficient is computed through its Green-Kubo expression

$$\eta = \int_0^\infty \eta(t)dt = \frac{\rho}{3k_B T} \sum \int_0^\infty \frac{\left\langle J^{xy}(0) J^{xy}(t) \right\rangle}{N} dt \qquad (5)$$

where the sum is to be made on the circular permutation of the indices xy. J^{xy} is the component of the microscopic stress tensor, given by

$$J^{xy}(t) = \sum_{i=1}^{N} \left(m v_i^x v_i^y - \frac{1}{2} \sum_{i\neq j} \frac{r_{ij}^x r_{ij}^y}{r_{ij}} \frac{\partial U(r_{ij})}{\partial r_{ij}} \right) \qquad (6)$$

where $\mathbf{v_i}$ are the particle velocities
Typical simulations runs correspond to 10000-20000 equilibration time steps followed by 50000 to 2 millions time steps during which the equilibrium properties and time dependent correlation functions are computed.

4. Results

4.1 Thermodynamic and transport quantities

Table 1: shows the average results for the following quantities: total energy E, pressure P, diffusion coefficients *D* and shear viscosity η. They are given in dimensionless reduced units: energies are divided by Nε, pressures by ε/σ^3, diffusion coefficients by $\sqrt{m/\varepsilon}\ /\ \sigma$ and shear viscosities by $\sigma^3/\varepsilon_{LJ}\tau$. For ease of comparison, available experimental data (exp)[5,20] are quoted.

State Point	System	T^*	ρ^*	Method	E*	P*	D^*	η^*	$2\beta\hbar^2/m\sigma^2$
sp1	Ne(l)	0.9517	0.6877	DMLJ	-3.41	-0.370	0.0967		
				QFH	-3.12	0.081	0.0989	1.190	0.01763
				Exp		0.093		1.430	
sp2	Ne(l)	0.9792	0.6938	DMLJ	-3.39	-0.309	0.1071		
				QFH	-3.10	0.206	0.1001	1.329	0.01713
				Exp	-3.03	0.135		1.370	

Table 1: Thermodynamical properties, energy, pressure, diffusion coefficients and shear viscosities for neon. ρ^*: reduced density. T^*: reduced temperature. E*: total energy in reduced units. P*: Pressure in reduced units. D^* : diffusion coefficients in reduced units. η^*: shear viscosity in reduced units . $2\beta\hbar^2/m\sigma^2$: quantum correction factor in the QFH potential. LJ and QFH results: this work; thermodynamical experimental data: Singer and Smith [5] ; and experimental shear viscosities : NIST[20].

FH quantum effects increase total energies as compared with the LJ values, the quantum potentials models giving less strongly bound fluids than LJ. At sp2, the agreement between the reported quantum total energies and the experiment is remarkably good. As regard quantum pressures, they are much better than the classical LJ estimates and close to the experimental values (sp1). At sp2, the FH pressures are, however, far from the experimental values. It turns out that the higher the density the larger are the pressure discrepancies.

As regards the diffusion coefficients values, there are no important differences between QFH and LJ. It is worth pointing out that the η values seem to be in good agreement with the experiment leading to QFH potentials that is η (QFH) ≤ η (exp). In addition, at sp1, the η behaviour can be understood by involving the low densities. From the foregoing results it can be concluded that: (a) the FH methods afford thermodynamic and transport properties remarkably close to experiment; (b) QFH and LJ approaches yield similar results, QFH being somewhat superior. The agreement deteriorates as the density increases, which can eventually lead to very poor estimates for some properties (e.g., pressure at sp2).

4.2 Pair distribution functions

The figure 1 presented in what follows is only illustrative of the data that can be obtained through our calculations ($r^* = r/\sigma$ denote distances in reduced units).

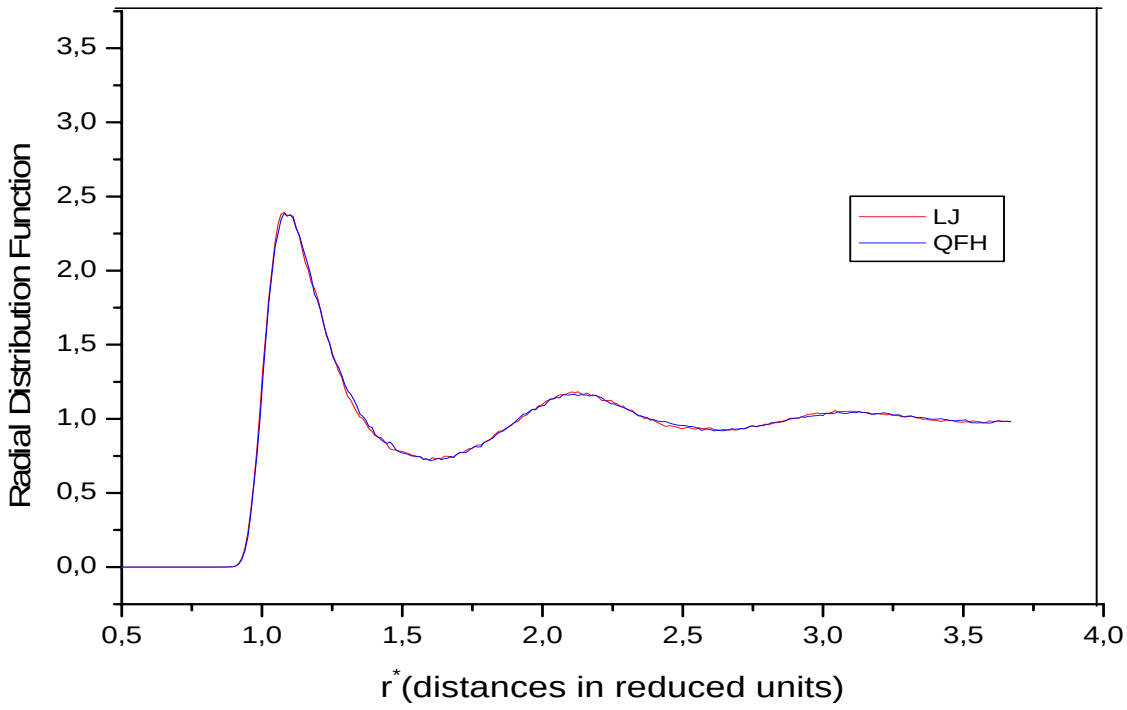

Figure 1: Classical (LJ) and quantum (QFH) pair distribution function for liquid neon at sp1 ($\rho^* = 0.6877$, $T^*=0.9517$).

On the scale of the graphs there are no significant differences between the LJ and QFH pair distribution functions. Figure 1 shows the relevant structural information for one representative point sp1 of liquid neon. The function g(r) becomes firstly zero at short distances, where repulsive forces prevent overlapping of molecules. When r is close to the collision diameter σ, g(r) increases rapidly to a maximum $r = r_m$ corresponding to the first peak. As r increases gradually, g(r) decreases showing that influence of the central molecule is disappearing and there is no order at long distances.

5. Conclusion

This paper has dealt with the Feynman-Hibbs potential (QFH) applied to the molecular dynamic simulation of liquid neon over a ρ, T range. The QFH thermodynamics and QFH shear viscosities obtained are in very good accordance with experiment. As seen in table 1, and putting aside the role played by a factor of corrections ($2\beta \hbar^2/ m\sigma^2$), the influence of P on the behaviour of the FH models is much more important than that of T. The QFH version appears to be better than LJ for computing thermodynamic quantities, as the latter is much too repulsive at short distances.
As regards the structural and the diffusion coefficients results, there are no important differences between QFH and LJ. In the light of the present results, it can be concluded that the reliability of the QFH potential is greater than the LJ potential.

References

1. J. P. Hansen and I.R. McDonald, *Theory of Simple Liquids* (London : Academic, **1986**).
2. Guggenheim, E. A. *J. Chem. Phys*. **1945**, *13*, 253.

3. Quantum exchange in liquid He^4 is significant at $T \leq 2K$; see Ceeperley, D. M., and Pollock, E, L. *Phys. Rev. Lett*. **1986**, *56*, 35.
4. Thirumalai, D., Hall, R. W., and Berne, B. J. *J. Chem. Phys*., **1984**, *81*, 2523.
5. Singer, K., and Smith, W. *Molec. Phys*., **1988**, *64*, 1215.
6. Wang, Q., Johnson, J. K., and Broughton, J. Q. *J. Chem. Phys.* **1997***, 107,*5108
7. Morales, J. J., and Singer, K. *Molec. Phys*., **1991**, *73*, 873.
8. Corbin, N., and Singer, K. *Molec. Phys*., **1982**, *46*, 671.
9. Singer, K., and Smith, W. *Molec. Phys*., **1986**, *57*, 761.
10. Hansen, J. P., and Weis, J. J. *Phys. Rev*., **1969**, *188*, 314.
11. Barocchi, F., Neumann, M., and Zoppi, M. *Phys. Rev*. A., **1987**, *36*, 2440 ; Neumann, M., and Zoppi, M. *Phys. Rev*. A., **1989**, *40*, 4572.
12. Powles, J. G., and Abascal, J. L. F. J. Phys. C., **1983**, *16*, L441.
13. Sesé, L. M. *Molec. Phys*., **1991**, *74*, 177.
14. Tchouar, N., Ould Kadour, F., and Levesque, D. *J. Chem. Phys*. **2004**, *121*, 7326
15. Guillot. B., and Guissani . Y. *J. Chem. Phys*. **1998**, *108*, 10162.
16. Feynman, R. P., and Hibbs, A., **1965**, Quantum Mechanics and Path-Integrals (McGraw-Hill) ; Feynman, R. P.,**1972**, Statistical Mechanics (Benjamin).
17. Sesé, L. M. *Molec. Phys*., **1992**, *76*, 1335.
18. Stratt, R. M. *J. Chem. Phys*. **1979**, *70*, 3630.
19. Allen, M.; and Tildesley, D. In *Computer Simulation of liquids* Oxford University Press : Oxford, 1987 .
20. NIST Chemistry WebBook online databases for fluid :(http://webbook.nist.gov/chemistry /fluid/)